Voltage Stability Analysis of Grid-Forming Converters with Current Limitation

Sebastian Liemann*, Christian Rehtanz
Institute of Energy Systems, Energy Efficiency and Energy Economics (ie³),
TU Dortmund University, Dortmund, Germany
*sebastian.liemann@tu-dortmund.de

***Abstract*—In this paper, a systematic short- and long-term voltage stability analysis of grid-forming converters with current limitations is conducted. For this, sampling studies are performed in an aggregated version of the Nordic test system. Here, the grid-forming control approach, the simulation type (EMT/phasor), current prioritisation and load composition are varied. Also, a stability-enhancing control method is developed to stabilise the converter during current limitation. The proposed method does not require any parameter tuning and can be applied to almost all grid-forming approaches. Its performance is demonstrated by comparing it to similar methods. The results show that the proposed method can greatly improve short- and long-term voltage stability for all investigated grid-forming approaches. In addition, accurate load models are crucial, as small modelling differences can have a greater impact on stability than the choice of simulation type. Here, both simulation types show the same voltage dynamics but have small differences in the stability limits.**

***Index Terms*—current limitation, EMT, grid-forming, stability-enhancing control method, voltage stability**

I. Introduction

Power electronic interfaced generation is changing the dynamics and stability of many power systems [1]. In this context, grid-forming (GFM) converters are considered a key solution to stabilise the grid if conventional power plants are decommissioned [2]. As their stabilising properties are often analysed for frequency and small-signal stability issues, less attention is given to their influence on voltage stability in case of large disturbances. Therefore, this paper tries to close this gap by analysing GFM converters in voltage-critical situations. First investigations about GFM converters and voltage stability have been carried out in [3] and [4]. The stabilizing effect of different shares of GFM generators on short-term voltage stability with phasor models has been investigated in [3]. Similarly, in [4] GFM and grid-following (GFL) converters are compared in a phasor simulation to investigate short-term voltage stability scenarios. However, none of these studies considers long-term dynamics or modelling variations in the GFM control. In general, GFM control can be classified into droop-based, synchronous-machine-based and other approaches, e.g. virtual oscillators [5]. As the selected GFM control approach has a decisive influence on stability, multiple approaches are considered in this paper. Since all of these controllers lead to voltage source characteristics, the current has to be limited to protect the converter [6]. As this causes a strong intervention in the GFM capabilities, the converter can lose its stable operating point during severe faults. To counteract this, various stability-enhancing control methods (SECMs) have been proposed [6]. Their general idea is to control the power reference values during current limitation to stay synchronised with the grid. However, some of these approaches need tuning of their parameters or have been developed for a specific type of GFM control. To remove these limitations, in this paper, a new SECM with an anti-windup method is presented, which can be used for almost all GFM approaches and does not need any tuning.

One question that arises along with many stability analyses is whether electromagnetic transient (EMT) or phasor models should be used. In [1] it is stated that phasor simulations are suitable for voltage stability investigations. This is also reflected by recent short-term [7]–[9] and long-term voltage stability investigations [10]–[12], however mostly done for GFL converters. In contrast, stability analyses of GFM converters are mainly conducted with EMT models. Here, frequency stability [13]–[15] and fault-ride through dynamics [16]–[19] are of major concern. Thus, it is not immediately obvious which model type should be selected. Therefore, the impact of the modelling type on voltage stability is also assessed in this paper. The main contributions of the paper are summarised below:

- Systematic simulative analyses of GFM converters for short- and long-term voltage stability by varying the GFM control approach, the simulation type (phasor/EMT), their current prioritisation in case of short circuits as well as the load compositions.
- Development of a universal parameter-free SECM and demonstration of its stabilisation effect compared to other SECMs.
- Derivation of a computationally efficient power system model, aggregated from the Nordic test system, for large sampling voltage stability studies as EMT and phasor simulation.

The rest of the paper is organised as follows. In Section II,

This work was funded by the Deutsche Forschungsgemeinschaft (DFG, German Research Foundation) - 360460668. Submitted to the 23rd Power Systems Computation Conference (PSCC 2024).

the utilised converter model, GFM controls as well as the developed SECM are summarised. In Section III, the voltage stability test system, aggregated from the Nordic test system as well as the stability assessment methods are described. In Section IV, the simulation results for assessing short and long-term voltage stability are presented. Finally, Section V comprises of conclusion and outlook.

II. Modelling Approach

In this section, the utilised converter model, the GFM control structures and the developed SECM are described. The converter model and GFM control structures are taken from [13], which were originally designed for EMT studies. Any adaptations to them are described in this section, e.g. to be suitable for phasor simulations. The selected controllers encompass a wide spectrum of GFM controls namely, droop control, matching control, dispatchable virtual oscillator control (dVOC) and a virtual synchronous machine (VSM).

A. Converter model and DC circuit

In this paper, the converter model is a symmetric average model with an RLC filter at the AC side, illustrated in Fig. 1. The DC circuit consists of a capacitance c_{dc}, a loss resistance r_{dc} and a controlled current source as an energy model. It is assumed that the energy source includes battery storage or represents one converter of a high-voltage direct current (HVDC) system. Thus, both configurations could provide a bidirectional power flow. The DC current reference value i_{dcref0} is calculated by

$$i_{\mathrm{dcref0}} = \frac{p_{\mathrm{ref}}}{v_{\mathrm{dc}}^*} + (v_{\mathrm{dc}}^* - v_{\mathrm{dc}})k_{\mathrm{dc}} + \frac{v_{\mathrm{dc}}}{r_{\mathrm{dc}}} + \frac{\Delta p_{\mathrm{c}}}{v_{\mathrm{dc}}^*} \tag{1}$$

where p_{ref} is the active power reference, k_{dc} a droop parameter, v_{dc}^* the nominal and v_{dc} the actual dc voltage. Also, the AC-filter losses are represented by the active power difference $\Delta p_{\mathrm{c}} = p_{\mathrm{c}} - p$ between the converter terminals ($p_{\mathrm{c}} = \Re(\underline{v}_{\mathrm{cdq}} \cdot \bar{\underline{i}}_{\mathrm{cdq}})$) and point of common coupling (PCC) ($p = \Re(\underline{v}_{\mathrm{dq}} \cdot \bar{\underline{i}}_{\mathrm{dq}})$). As the DC energy source can only provide a current in a certain range, it is limited by $\pm i_{\mathrm{dcmax}}$. Additionally, its shift to a new setpoint is delayed by the time constant T_{dc}. The coupling between DC and AC power is given by

$$i_{\mathrm{dc}} = \frac{p_{\mathrm{c}}}{v_{\mathrm{dc}}} = \frac{\Re(\underline{v}_{\mathrm{cdq}} \cdot \bar{\underline{i}}_{\mathrm{cdq}})}{v_{\mathrm{dc}}}, \tag{2}$$

and the terminal voltage $\underline{v}_{\mathrm{cdq}}$ is linked with the DC side by

$$\underline{v}_{\mathrm{cdq}} = \underline{v}_{\mathrm{cdqm}} \cdot \frac{v_{\mathrm{dc}}}{v_{\mathrm{dc}}^*}, \tag{3}$$

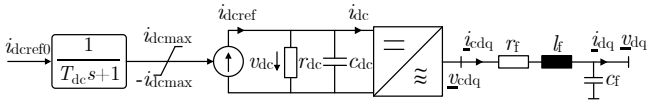

Fig. 1: Converter model with DC energy model and AC filter (own illustration, based on [13])

with $\underline{v}_{\mathrm{cdqm}}$ as the modulation voltage. For the phasor models, the DC circuit is modelled in such a way that only the DC voltage deviation Δv_{dc} from its nominal value is considered.

B. Cascaded control and current limitation

For the low-level control, a state-of-the-art cascaded voltage and current loop in the dq-reference frame is taken and shown in Fig. 2. The reference voltage is $\underline{v}_{\mathrm{dq}}$ at the PCC. For the dq-transformation inside the GFM control the angle θ from the power synchronisation loop is taken so that in steady-state $v_{\mathrm{q}} = 0$ results. It has to be noted that in the EMT simulations the filter impedances x_{cf} and x_{lf} are calculated by the angular frequency ω of the GFM control, whereas for phasor models, the base value ω_0 is taken. In case the absolute value of the current reference $|\underline{i}_{\mathrm{cdqref}}|$ exceeds its maximum value i_{cmax}, it is limited to $\underline{i}_{\mathrm{cdqlim}}$. Here, it can be selected whether the current is scaled down without any axis prioritisation (which is the default case)

$$\underline{i}_{\mathrm{cdqlim}} = \begin{cases} \underline{i}_{\mathrm{cdqref}} \frac{i_{\mathrm{cmax}}}{|\underline{i}_{\mathrm{cdqref}}|} & \text{if } |\underline{i}_{\mathrm{cdqref}}| \geq i_{\mathrm{cmax}}, \\ \underline{i}_{\mathrm{cdqref}} & \text{if } |\underline{i}_{\mathrm{cdqref}}| < i_{\mathrm{cmax}} \end{cases} \tag{4}$$

or the q-axis current is prioritised (and $|\underline{i}_{\mathrm{cdqref}}| \geq i_{\mathrm{cmax}}$ holds)

$$i_{\mathrm{cqlim}} = \begin{cases} i_{\mathrm{cqref}} & \text{if } |i_{\mathrm{cqref}}| < i_{\mathrm{cmax}}, \\ \mathrm{sgn}(i_{\mathrm{cqref}}) \cdot i_{\mathrm{cmax}} & \text{if } |i_{\mathrm{cqref}}| \geq i_{\mathrm{cmax}}, \end{cases} \tag{5}$$

$$i_{\mathrm{cdlim}} = \begin{cases} i_{\mathrm{cdref}} & \text{if } |i_{\mathrm{cdref}}| < \gamma_{\mathrm{dlim}}, \\ \mathrm{sgn}(i_{\mathrm{cqref}}) \cdot \gamma_{\mathrm{dlim}} & \text{if } |i_{\mathrm{cdref}}| \geq \gamma_{\mathrm{dlim}}, \end{cases} \tag{6}$$

with $\gamma_{\mathrm{dlim}} = \sqrt{i_{\mathrm{cmax}}^2 - i_{\mathrm{cqlim}}^2}$. In case the current is limited, an anti-windup signal is sent to the PI voltage controllers to set the input of the integrator to zero, which is not part of the original implementation in [13], but used for the developed SECM which is described in more detail in Section II-D.

C. Grid-forming controls

Next, the utilised GFM controls, droop, matching, dVOC and VSM are described. The inputs p_{meas}, q_{meas}, $\underline{v}_{\mathrm{dq}}$ and $\underline{i}_{\mathrm{dq}}$ are measured from the PCC and $\underline{i}_{\mathrm{cdq}}$ at the converter's terminal. The controllers are illustrated in Fig. 3.

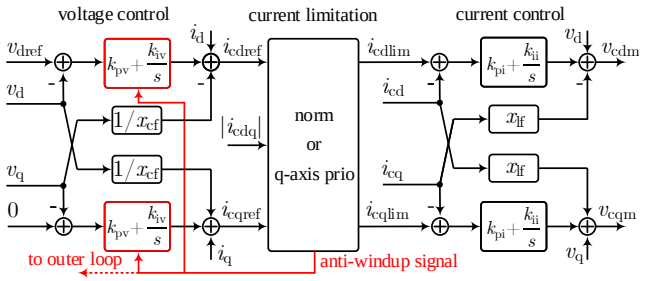

Fig. 2: Cascaded voltage and current control with current limitation and anti-windup method (own illustration, based on [13])

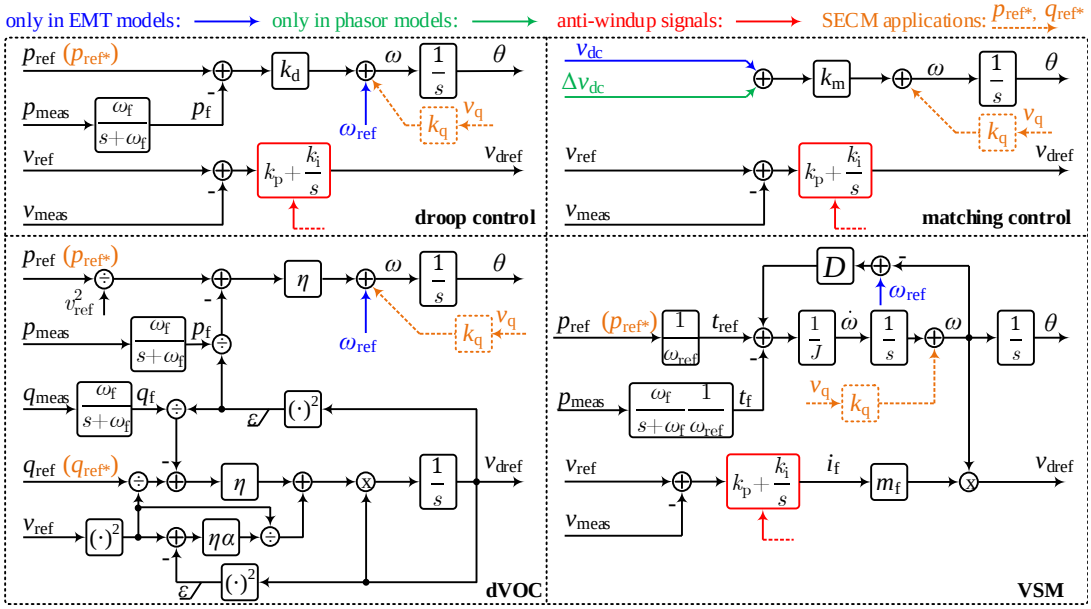

Fig. 3: Utilised GFM controls, highlighting simulation type differences as well as anti-windup and SECM applications (own illustration, based on [13])

1) droop control: Due to its simplicity, droop control is a well-known GFM approach. Its angle dynamics are given by

$$\dot{\theta} = \omega = \omega_{\mathrm{ref}} + (p_{\mathrm{ref}} - p_{\mathrm{f}})k_{\mathrm{d}} \tag{7}$$

with k_{d} as droop parameter, p_{f} as filtered measured active power and ω_{ref} as angular frequency reference (only in EMT models). For voltage control, a basic PI control is used, described by

$$\begin{aligned} \dot{x}_{\mathrm{v}} &= (v_{\mathrm{ref}} - v_{\mathrm{meas}})k_{\mathrm{i}} \\ v_{\mathrm{dref}} &= x_{\mathrm{v}} + (v_{\mathrm{ref}} - v_{\mathrm{meas}})k_{\mathrm{p}} \end{aligned} \tag{8}$$

where k_{p} and k_{i} are the proportional and integral gain. Here and for the other GFM approaches the described anti-windup is also used for the PI voltage controller by setting $\dot{x}_{\mathrm{v}} = 0$ in case of current limitation.

2) matching control: Matching control is based on the structural similarities of power balance between the electromechanical part of a synchronous generator with its turbine and a converter DC circuit with its capacitance. Here, a power imbalance is detected as a DC voltage deviation. Therefore, the DC voltage v_{dc} is used to determine the angle dynamics

$$\dot{\theta} = \omega = v_{\mathrm{dc}}k_{\mathrm{m}} \tag{9}$$

where k_{m} is a parameter that has to be set to match the desired angular frequency. For phasor simulations, only the DC voltage deviation Δv_{dc} is taken, as only the deviation of the angular frequency $\Delta\omega$ is needed. Like the droop control, voltage control is realised by a PI controller as in (8).

3) dispatchable virtual oscillator control: The dVOC is derived from the theory of coupled harmonic oscillators to operate in parallel with other converters. The power synchronisation principle and angle dynamics $\dot{\theta}$ are described by

$$\dot{\theta} = \omega = \omega_{\mathrm{ref}} + \eta\left(\frac{p_{\mathrm{ref}}}{v_{\mathrm{ref}}^2} - \frac{p_{\mathrm{f}}}{v_{\mathrm{dref}}^2}\right) \tag{10}$$

where η is a control parameter and v_{ref} the reference voltage. For phasor simulations, ω_{ref} is neglected. The reactive and voltage control loop is given by

$$\dot{v_{\mathrm{dref}}} = v_{\mathrm{dref}}\left(\eta\left(\frac{q_{\mathrm{ref}}}{v_{\mathrm{ref}}^2} - \frac{q_{\mathrm{f}}}{v_{\mathrm{dref}}^2}\right) + \beta\left(v_{\mathrm{ref}}^2 - v_{\mathrm{dref}}^2\right)\right) \tag{11}$$

whith $\beta = (\eta\alpha)/(v_{\mathrm{ref}}^2)$ and α as a control parameter and q_{f} as the filtered reactive power.

4) virtual synchronous machine control: While matching control is only inspired by the similarities of power synchronisation in a synchronous generator, the VSM tries to emulate it by the swing equation

$$\ddot{\theta} = \dot{\omega} = \frac{1}{J}\left(t_{\mathrm{ref}} - t_{\mathrm{f}} + D(\omega_{\mathrm{ref}} - \omega)\right) \tag{12}$$

where J is the virtual inertia parameter and D the damping factor. Here, the power signals p_{ref} and p_{meas} are converted into their torque values t_{ref} and t_{f} by dividing them with ω_{ref}. Similar to the droop and matching control, a PI controller is used for voltage control. The difference is that a virtual mutual impedance m_{f} and the angular frequency ω are used to emulate an automatic voltage regulator (AVR) (see [13]).

D. Stability-enhancing control methods

First, the proposed SECM is introduced, which is called SECM-1 here. Second, the other SECMs are described which serve as a benchmark. It has to be noted that for all SECMs the above-described anti-windup strategy is applied, which is not part of their original implementation (except SECM-3) but increases their stabilising effect. To avoid algebraic loops the output of all SECMs are filtered by a first-order lag system with a time constant of 10^{-4} s. Also, they are limited by the maximum rated apparent power of the converter (except SECM-3). If not stated otherwise, the default parameter value for each SECM based on the given references is taken.

1) SECM-1: p_{ref} and q_{ref} adaptation based on $\underline{i}_{\mathrm{cdqlim}}$: In case of current limitation, the maximum active and reactive power injection of the converter depends on maximum converter current i_{cmax} and the PCC voltage $\underline{v}_{\mathrm{dq}}$. Thus, if the active power reference p_{ref} would be bigger, the angle θ increases continuously and the converter is no longer synchronised. Therefore, a SECM approach is proposed in this paper which changes the active power reference in the event of current limitation (see (4)) according to the limited current reference $\underline{i}_{\mathrm{cdqlim}} = i_{\mathrm{cdlim}} + \mathrm{j}i_{\mathrm{cqlim}}$ and the voltage $\underline{v}_{\mathrm{dq}}$:

$$\begin{aligned} p^*_{\mathrm{ref}} &= v_{\mathrm{d}} \cdot i_{\mathrm{cdlim}} + v_{\mathrm{q}} \cdot i_{\mathrm{cqlim}}, \\ q^*_{\mathrm{ref}} &= v_{\mathrm{q}} \cdot i_{\mathrm{cdlim}} - v_{\mathrm{d}} \cdot i_{\mathrm{cqlim}} + \frac{|\underline{v}_{\mathrm{dq}}|^2}{x_{\mathrm{cf}}}. \end{aligned} \tag{13}$$

By this, the power reference values follow the output of the current limitation and the converter stays synchronised. Matching control is also affected by this approach, as the DC energy model also includes p_{ref} (cf. (1)). As the reactive power at the PCC also depends on the filter capacitance, its reactive power share is respected in (13). This parameter-free SECM is completed by the above-described anti-windup for the PI controllers at the outer and inner voltage control.

2) SECM-2: p_{ref} adaptation based on $|\underline{v}_{\mathrm{dq}}|$: In [20] a linear adaptation of the active power reference based on the per unit voltage $|\underline{v}_{\mathrm{dq}}|$ is presented and described by

$$p^*_{\mathrm{ref}} = \begin{cases} p_{\mathrm{ref}} & \text{if } |\underline{v}_{\mathrm{dq}}| \geq 0.9 \text{ pu}, \\ p_{\mathrm{ref}} \cdot |\underline{v}_{\mathrm{dq}}| & \text{if } |\underline{v}_{\mathrm{dq}}| < 0.9 \text{ pu}. \end{cases} \tag{14}$$

Thus, SECM-2 is only activated at low and not around nominal voltages.

3) SECM-3: stability-enhanced component: In [17] a stability-enhanced component is introduced, which adds a damping term $\Delta\omega$ on the angular frequency ω, consisting of v_{q} multiplied by the factor $k_{\mathrm{q}} = 5$. As v_{q} is zero in steady-state, it damps the acceleration of θ only during transients. Originally it has been only designed for $P - f$ droop control, but can also be used for other GFM approaches (see orange dotted lines in Fig. 3)

$$\Delta\omega = v_{\mathrm{q}} \cdot k_{\mathrm{q}}. \tag{15}$$

4) SECM-4: p_{ref} adaptation based on current-droop: In [13] a SECM is presented where the active power reference is decreased by a droop characteristic of $\underline{i}_{\mathrm{cdq}}$ in case of current limitation

$$p^*_{\mathrm{ref}} = \begin{cases} p_{\mathrm{ref}} & \text{if } |\underline{i}_{\mathrm{cdq}}| < i_{\mathrm{thr}}, \\ p_{\mathrm{ref}} - \gamma(|\underline{i}_{\mathrm{cdq}}| - i_{\mathrm{thr}}) & \text{if } |\underline{i}_{\mathrm{cdq}}| \geq i_{\mathrm{thr}}, \end{cases} \tag{16}$$

where $\gamma = 2.3$ is the droop parameter and $i_{\mathrm{thr}} = 0.92\,\mathrm{pu}$ is the current threshold for activation. Here, the question arises of how to parametrise i_{thr} and γ for a proper stabilisation.

III. Aggregated Nordic System (ANS) and Voltage Stability Assessment Methods

The Nordic test system is a well-known grid for investigating voltage stability [21]. To derive a voltage stability test system that can also be easily used for large-sampling EMT simulations, an Aggregated Nordic System (ANS) is proposed in this paper. In this way, the computational complexity is reduced and the essential voltage dynamics are preserved. Also, the conventional generation can be easily replaced by GFM converters to investigate their impact. A MATLAB Simulink EMT implementation with all grid and control parameters is available online at [22]. For the phasor simulations, the grid is modelled with *PowerDynamics.jl* [23] and solved by *DifferentialEquations.jl* [24]. Next, the aggregation procedure is outlined.

The original Nordic test system structure consists of two main generation areas (External and North) and two load areas (Central and South), which is mainly preserved for the ANS (see Fig. 4). The first step of building the ANS is the aggregation of the main generation area (green). As the voltages in this area stay around nominal values they are represented in the ANS by a constant voltage source with v_0. However, to represent its limited short-circuit contribution in case of a fault, a grid impedance $\underline{z}_{\mathrm{g}}$ is introduced. Here, the voltage v_0 and grid impedance $\underline{z}_{\mathrm{g}}$ are chosen in such a way that they match the sub-transient short-circuit power S''_{k} at bus 4031 in the Nordic test system. By this, the initial voltage of v_1 in the ANS is nearly the same as that of bus 4031. In the second step, the long transmission lines between the North and Central areas are connected in parallel and aggregated into one line, except the line between bus 4032 and 4044. This line is modelled without any changes, to emulate the original fault and its subsequent disconnection. To match the voltage drop in the load area during the short circuit, the fault position is at a 10 % distance to bus 2. In the last step, the load, generation and shunt capacitors in the central and south areas are aggregated and connected via transformers T2 and T3 at the 130 kV level. The shunt capacitors are aggregated for the 400 kV and 130 kV buses separately. Here, T3 is equipped with an on-load tap changer (OLTC) at the secondary side. To emulate the voltage dependency of the load (linear for active and quadratic for

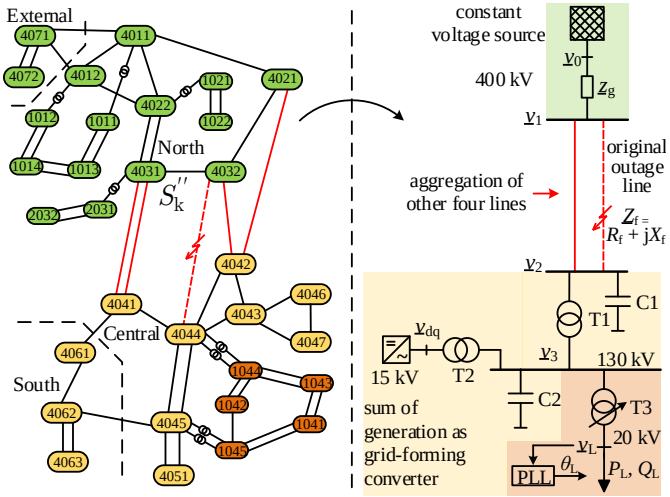

Fig. 4: Aggregation procedure of the Nordic test system to the ANS

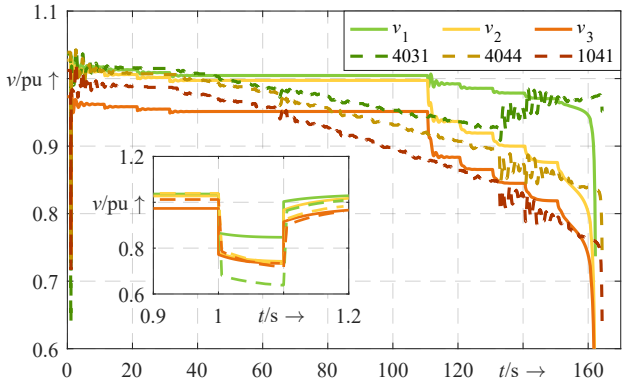

Fig. 5: Comparison of voltage dynamics between Nordic test system and ANS in a phasor simulation (for synchronous generators)

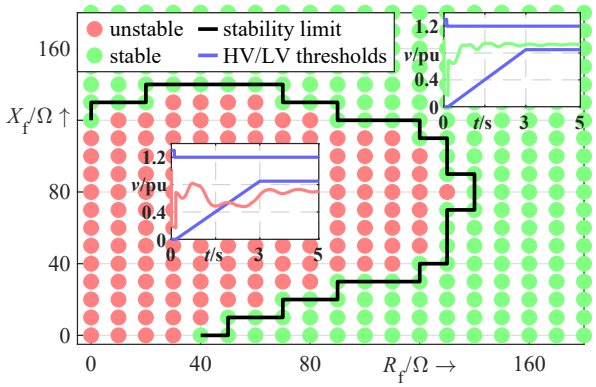

Fig. 6: Exemplary determination of a short-term voltage stability limit by short-circuit impedance sampling ($|\Delta X_\mathrm{f}| = |\Delta R_\mathrm{f}| = 10\,\Omega$) and assessing high and low-voltage stability thresholds

reactive power) in the EMT model, the active power part is modelled as a constant current source which is synchronised by a phase-locked loop (PLL) in $\alpha\beta$-coordinates tracking the voltage angle of $\underline{v}_\mathrm{L}$. The PLL control parameters are taken from [25]. All other grid and control parameters can be found in [22] and the appendix of this paper. A comparison of the voltage dynamics of the original system and the ANS is shown in Fig. 5. Although the voltage oscillations are reduced in the ANS and the dynamics mainly depend on the single generator and OLTC, similar voltage collapse times are obtained. Also, the heights of the voltage drops are comparable during the short circuit in the main load area, which is of main interest here.

To assess short-term voltage stability, high-voltage (HV) and low-voltage (LV) thresholds of fault ride-through requirements from [26] are taken. The system is labelled as unstable if the thresholds are violated during a 5 s simulation time. To determine the stability limit of different GFM controls, SECMs and grid scenarios, sampling studies are carried out by varying the short-circuit impedance $\underline{Z}_\mathrm{f} = R_\mathrm{f} + jX_\mathrm{f}$ with a fixed short-circuit duration of 0.1 s. The resolution of the impedance sampling is given by $|\Delta X_\mathrm{f}|$ and $|\Delta R_\mathrm{f}|$. By this, the stability limit for each setup can be determined. In Fig. 6 an exemplary representation of the determination of a short-term voltage stability limit by short-circuit impedance sampling is illustrated. For the sake of simplicity, only the stability limits are used in the following result figures. For long-term voltage stability analysis, a time-domain comparison is conducted.

IV. Simulation Results

In this section, the short and long-term voltage stability results for different GFM controls and SECMs are presented.

A. Short-term voltage stability

For the short-term voltage stability assessment, first, the influence of load compositions and the simulation type is examined. Second, the impact of the introduced SECMs on different GFM approaches is analysed. The assessment is concluded with an investigation of the q-axis current prioritisation in combination with the SECMs.

1) Voltage dependency of loads: Fig. 7 illustrates the different stability limits of a droop converter for different load compositions and simulation types without any SECM. Here, e.g. $p_\mathrm{L,I} = 0.9$ means that 90 % of the load's active power is modelled as a constant current and 10 % as a constant resistance. For this scenario, only the droop control is shown, as the results of the other GFM controls have no qualitative difference. In general, a higher share of constant resistance load leads to a more stable system. Also, the phasor model has mostly a slightly higher stability limit. However, as can be seen from the results a minor increase of constant resistance by 1 % has a bigger impact on stability than the simulation type. This means for this grid that the load composition is more sensitive regarding the stability limit than choosing between the EMT load model (constant current source + PLL dynamics) or the phasor load model (algebraic equation).

2) Impact of different SECMs in case of short circuits: Next, a comparison is made regarding the different SECMs on the four GFM controls (see Fig. 8). As the results show, SECM-1 increases stability at most. Only for the VSM, SECM-2 leads to a higher increase than SECM-1. In contrast, the effect of SECM-3 and SECM-4 varies more between the GFM controls, but SECM-3 has for all GFM controls the least stabilising impact. Comparing the GFM controls, it can

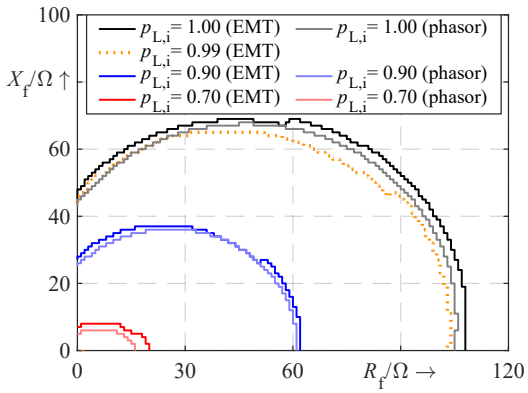

Fig. 7: Short-term voltage stability limits of a droop converter for different load compositions and simulation type ($|\Delta X_\mathrm{f}| = |\Delta R_\mathrm{f}| = 1\,\Omega$)

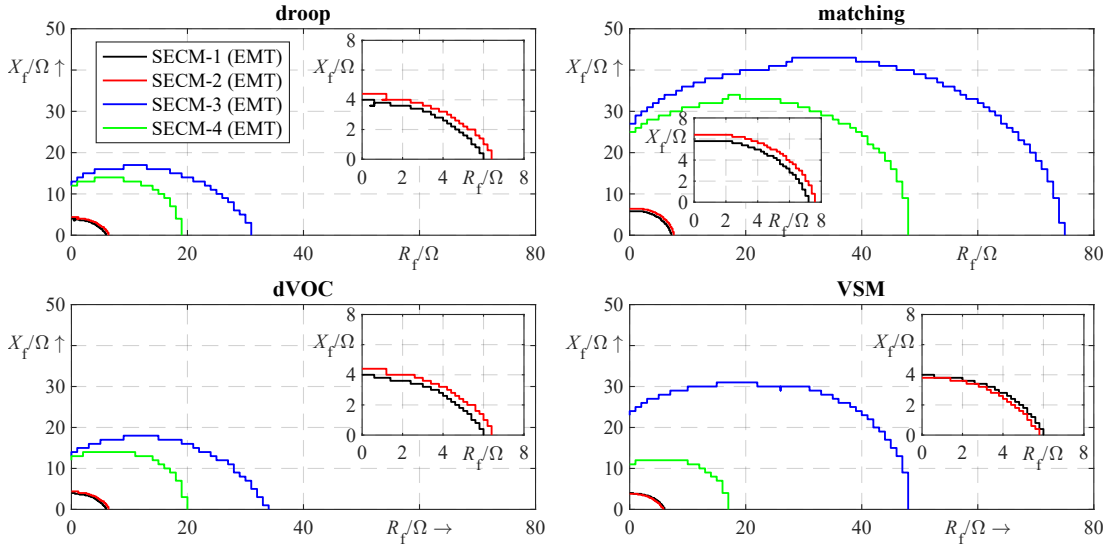

Fig. 8: Short-term voltage stability limits for four GFM controls, four SECMs and pure constant current active power load ($p_{\mathrm{L,I}} = 1.0$) ($|\Delta X_\mathrm{f}| = |\Delta R_\mathrm{f}| = 0.2\,\Omega$ for SECM-1 and SECM-2; $|\Delta X_\mathrm{f}| = |\Delta R_\mathrm{f}| = 1\,\Omega$ for SECM-3 and SECM-4)

be seen that the droop and dVOC are very similar regarding their stability limit, whereas matching and VSM vary more. In summary, all SECMs can improve the stability limit (cf. Fig.7 for $p_{\mathrm{L,I}} = 1.0$), but SECM-1 and SECM-2 clearly stand out.

3) Impact of q-axis current prioritisation: Fig. 9 shows the stability limits in the case of a q-axis current prioritisation for SECMs. In general, the q-axis current prioritisation leads to a lower stability limit. The main reason is that the converter injects more reactive power than active power and thus does not meet the requested active power of the load. Hence, q-axis current prioritisation is not effective in this grid, which is also reflected by the SECMs where most of them are comparable according to their stability limit, except SECM-3. However, this can be different for other grids.

B. Long-term voltage stability

In the following, the impact of the current limitation of GFM converters on long-term voltage stability is analysed. As the ANS is long-term stable with the original GFM converter, its rated power is decreased by around 3 % (from 5300 MVA to 5142 MVA) to demonstrate some of its specific dynamics. Due to the higher steady-state current i_thr is increased to 0.95 for SECM-4. At first, it is shown how the converter responds in case it hits its current limitation if an OLTC recovers the load voltage. Second, the described SECMs are added to the scenario. Here, only the droop control is shown as the other GFM controls show a qualitatively similar response.

In Fig. 10 a time-domain comparison of a droop converter without SECM is shown for the EMT and phasor model. Here, the line outage is without a short circuit due to the short-term instability of the converter. It can be seen that the voltages collapse at the time the converter hits its current limitation. This is caused by the converter which cannot inject its active power reference anymore and thus increases its angle θ continuously and is no longer synchronised with the grid. Therefore, the main cause of this voltage drop is the desynchronisation of the converter. The EMT and phasor models generally show the same response, but the voltage collapse occurs two seconds later in the latter. Overall, this scenario shall demonstrate that a GFM converter can become unstable and induce voltage instability in case of current limitation at nearly nominal voltages. Next, the same scenario but with SECMs is presented. As seen in Fig. 11 all SECMs

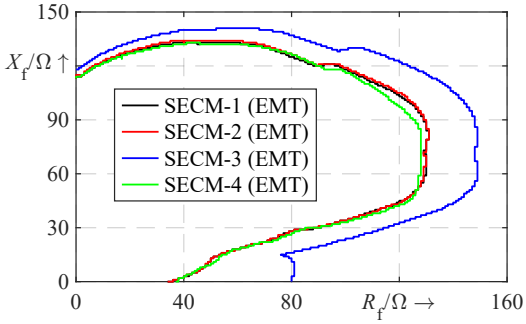

Fig. 9: Short-term voltage stability limits of a droop converter with q-axis current prioritisation for four SECMs and $p_{\mathrm{L,I}} = 1.0$ ($|\Delta X_\mathrm{f}| = |\Delta R_\mathrm{f}| = 1\,\Omega$)

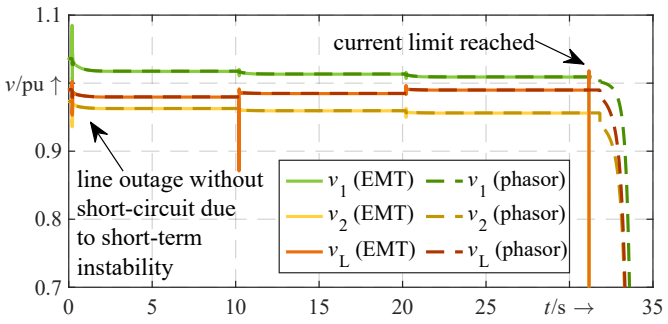

Fig. 10: Time-domain comparison of long-term voltage dynamics for an EMT and phasor model of a droop converter without SECM and $p_{\mathrm{L,I}} = 1.0$

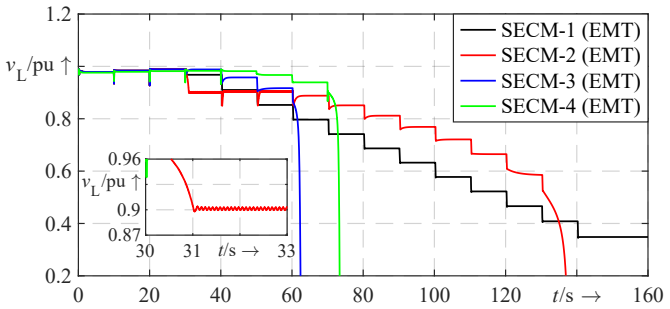

Fig. 11: Comparison of long-term voltages dynamics of the load voltage v_L for a droop converter with four different SECM and $p_{L,I} = 1.0$

can stabilise the converter during current limitation at $t \approx 31$ s. Here, SECM-3 and SECM-4 can keep the voltage at higher values first but become unstable around $t \approx 62$ s and $t \approx 73$ s. In the case of SECM-2, current limitation leads at first to a chattering around its activation voltage of 0.9 pu until the voltage drops lower after three additional OLTC taps. In addition, it gets unstable around $t \approx 136$ s too. Although the voltage is lower for SECM-1, it stabilises the converter during the whole simulation even at extremely low voltages until the OLTC has reached its final tap position. Here, it should be considered that the main task of a SECM is to keep the converter stable and should not compensate for the destructive action of other equipment like frequent OLTC tapping.

V. Conclusion

A systematic voltage stability analysis of GFM converters in an aggregated Nordic test system has been conducted. As the results show, GFM converters can become short or long-term unstable in case of current limitation in voltage-critical grids. As a countermeasure, SECMs control the active power reference during current limiting and, in combination with an anti-windup, effectively stabilise the converter. However, their effectiveness depends on the GFM control and stability scenario. In this regard, SECM-1 has been introduced, which is capable of stabilising various GFM controls in the short and long term effectively without any parameter tuning. Besides, accurate load modelling, especially its voltage dependence, is still one of the most important aspects of voltage stability, as it has a high impact but its exact composition is often unknown. Finally, the comparison between EMT and phasor models indicates that the same fundamental voltage dynamics occur but with small deviations around the stability limit, which could be induced by load model differences, e.g. of the load's active power.

Acknowledgement

The authors gratefully acknowledge the computing time provided on the Linux HPC cluster at Technical University Dortmund (LiDO3), partially funded in the course of the Large-Scale Equipment Initiative by the Deutsche Forschungsgemeinschaft (DFG, German Research Foundation) as project 271512359.

References

[1] N. Hatziargyriou *et al.*, "Definition and classification of power system stability – revisited & extended," *IEEE Transactions on Power Systems*, vol. 36, no. 4, pp. 3271–3281, jul 2021.

[2] F. Milano, F. Dorfler, G. Hug, D. J. Hill, and G. Verbič, "Foundations and challenges of low-inertia systems (Invited Paper)," *20th Power Systems Computation Conference, PSCC 2018*, pp. 1–25, 2018.

[3] M. Herrmann and L. Hofmann, "Ensuring short-term voltage stability in extensive grids with high power electronic penetration by applying grid forming controls," *Proceedings - 2020 International Conference on Smart Grids and Energy Systems, SGES 2020*, vol. 7, pp. 24–29, 2020.

[4] M. Coumont, B. Braun, and J. Hanson, "Influence of grid-forming inverter control on short-term voltage stability in distribution grids," *18th Wind Integration Workshop*, 2019.

[5] D. B. Rathnayake *et al.*, "Grid forming inverter modeling, control, and applications," *IEEE Access*, vol. 9, pp. 114 781–114 807, 2021.

[6] X. Wang, M. G. Taul, H. Wu, Y. Liao, F. Blaabjerg, and L. Harnefors, "Grid-synchronization stability of converter-based resources — an overview," *IEEE Open Journal of Industry Applications*, vol. 1, no. September, pp. 115–134, 2020.

[7] S. Stankovic, T. Van Cutsem, and L. Soder, "Fault-current injection strategies of inverter-based generation for fast voltage recovery," *IEEE Transactions on Power Systems*, vol. 37, no. 2, pp. 1543–1553, 2022.

[8] A. Boričić, J. L. R. Torres, and M. Popov, "Fundamental study on the influence of dynamic load and distributed energy resources on power system short-term voltage stability," *International Journal of Electrical Power and Energy Systems*, vol. 131, no. January, 2021.

[9] M. Jiang, Q. Guo, H. Sun, and H. Ge, "Short-term voltage stability-constrained unit commitment for receiving-end grid with multi-infeed HVDCs," *IEEE Transactions on Power Systems*, vol. 36, no. 3, pp. 2603–2613, 2021.

[10] L. D. P. Ospina and T. Van Cutsem, "Emergency support of transmission voltages by active distribution networks: a non-intrusive scheme," *IEEE Transactions on Power Systems*, vol. 36, no. 5, pp. 3887–3896, 2021.

[11] K. D. Dharmapala, A. Rajapakse, K. Narendra, and Y. Zhang, "Machine learning based real-time monitoring of long-term voltage stability using voltage stability indices," *IEEE Access*, vol. 8, 2020.

[12] L. Robitzky, T. Weckesser, U. Häger, C. Rehtanz, and T. V. Van Cutsem, "Agent-based identification and control of voltage emergency situations," *IET Generation, Transmission and Distribution*, vol. 12, no. 6, pp. 1446–1454, 2018.

[13] A. Tayyebi, D. Groß, A. Anta, F. Kupzog, and F. Dörfler, "Frequency stability of synchronous machines and grid-forming power converters," *IEEE Journal of Emerging and Selected Topics in Power Electronics*, vol. 8, no. 2, pp. 1004–1018, 2020.

[14] R. H. Lasseter, Z. Chen, and D. Pattabiraman, "Grid-forming inverters: a critical asset for the power grid," *IEEE Journal of Emerging and Selected Topics in Power Electronics*, vol. 8, no. 2, pp. 925–935, 2020.

[15] C. Li, Y. Yang, N. Mijatovic, and T. Dragicevic, "Frequency stability assessment of grid-forming VSG in framework of MPME with feed-forward decoupling control strategy," *IEEE Transactions on Industrial Electronics*, vol. 69, no. 7, pp. 6903–6913, 2022.

[16] J. Chen, F. Prystupczuk, and T. O'Donnell, "Use of voltage limits for current limitations in grid-forming converters," *CSEE Journal of Power and Energy Systems*, vol. 6, no. 2, pp. 259–269, 2020.

[17] L. Huang et al., "Transient stability analysis and control design of droop-controlled voltage source converters considering current limitation," *IEEE Transactions on Smart Grid*, vol. 10, no. 1, pp. 578–591, 2019.

[18] T. Qoria, F. Gruson, F. Colas, X. Kestelyn, and X. Guillaud, "Current limiting algorithms and transient stability analysis of grid-forming VSCs," *Electric Power Systems Research*, vol. 189, 2020.

[19] D. Pan, X. Wang, F. Liu, and R. Shi, "Transient stability of voltage-source converters with grid-forming control: a design-oriented study," *IEEE Journal of Emerging and Selected Topics in Power Electronics*, vol. 8, no. 2, pp. 1019–1033, 2020.

[20] N. Wiese, D. Duckwitz, M. Nuschke, Y. Zhang, and M. Braun, "Fault operation of grid-forming converters with focus on system stability," *11th Solar & Storage Power System Integration Workshop (SIW 2021)*, pp. 65–70, 2021.

[21] T. Van Cutsem et al., "Test systems for voltage stability studies," *IEEE Transactions on Power Systems*, vol. 35, no. 5, pp. 4078–4087, 2020.

[22] S. Liemann and C. Rehtanz, "Implementation of the aggregated nordic system with a grid-forming converter," Github, 2024. [Online]. Available: https://github.com/SLiemann/Aggregated-Nordic-System-with-GFM
[23] A. Plietzsch *et al.*, "Powerdynamics.jl—an experimentally validated open-source package for the dynamical analysis of power grids," *SoftwareX*, vol. 17, 2022.
[24] C. Rackauckas and Q. Nie, "Differentialequations.jl–a performant and feature-rich ecosystem for solving differential equations in julia," *Journal of Open Research Software*, vol. 5, no. 1, p. 15, 2017.
[25] Z. Ali, N. Christofides, L. Hadjidemetriou, E. Kyriakides, Y. Yang, and F. Blaabjerg, "Three-phase phase-locked loop synchronization algorithms for grid-connected renewable energy systems: A review," *Renewable and Sustainable Energy Reviews*, vol. 90, pp. 434–452, 2018.
[26] Forum Netztechnik / Netzbetrieb im VDE, "VDE-AR-N 4131 - Technical requirements for grid connection of high voltage direct current systems and direct current-connected power park modules (TAR HVDC)," Mar. 2019.

APPENDIX

Note that the unit values apply to the base values given within each table. A MATLAB Simulink-R2021b (EMT) and PowerDynamics.jl (phasor) implementation can be found in [22].

TABLE I: Technical data of ANS

Parameter	Value
S_{base}	8000 MVA
V_{base}	400 kV
$\lvert\underline{v}_0\rvert$	1.05428 pu
$\underline{z}_{\text{g}}$	0.075704 + j0.86229 pu
$x_{\text{L,aggregated}}$	j0.87427 pu
$r_{\text{aggregated}}$	0.15701 pu
$x_{\text{C/2,aggregated}}$	- j16.33192 pu
$x_{\text{L,original}}$	4.0 pu
r_{original}	0.48 pu
$x_{\text{C/2,original}}$	-j66.73162 pu
Q_{C1}	-600 MVAr
Q_{C2}	-850 MVAr
P_{L}	7580 MW
Q_{L}	2243.7 MVAr
k_{P}(PLL)	92 pu
k_{I}(PLL)	4255.3 pu

TABLE II: Technical data of transformers within ANS

Name	S_{base}	V_{HV}	V_{LV}	u_{k}	R/X
T1	8000 MVA	1.05·400 kV	130 kV	0.12 pu	0
T2	5300 MVA	1.05·130 kV	15 kV	0.15 pu	0
T3	8000 MVA	130 kV	20 kV	0.11 pu	0

TABLE III: Technical data of OLTC (T3) within ANS

min. tap	max. tap	initial tap	Δv	v_{ref}	deadband	τ
0	20	6	0.01 pu	1.0 pu	±0.01 pu	10 s

TABLE IV: Model parameters of GFM converter, AC Filter and DC energy source model (values taken from [13])

Parameter	Value
S_{base}	5300 MVA
V_{base}	15 kV
S_{rated}	5300 MVA
P_{ref}	4440 MW
v_{ref}	1.0 pu
i_{cmax}	1.0 pu
i_{dcmax}	1.2 pu
r_{dc}	20 pu
c_{dc}	0.096 pu
T_{dc}	0.05 s
k_{dc}	100 pu
r_{f}	0.0005 pu
x_{lf}	0.031416 pu
x_{cf}	5.305165 pu

TABLE V: Control parameters of the four power synrchronisation and outer voltage controls

	k_{d}	ω_{f}	k_{p}	k_{i}	
droop	π pu	$100\pi\ \frac{1}{\text{s}}$	0.5 pu	0.001 pu	
	k_{m}	k_{p}	k_{i}		
matching	100π pu	0.5 pu	0.001 pu		
	η	ω_{f}	α	ϵ	
dVOC	π pu	$100\pi\ \frac{1}{\text{s}}$	66666.666 pu	10^{-9} pu	
	D	J	ω_{f}	k_{p}	k_{i}
VSM	100 pu	2 pu	$100\pi\ \frac{1}{\text{s}}$	0.5 pu	0.001 pu
	m_{f}				
	1.0 pu				

TABLE VI: Control parameters of inner voltage and current control (values taken from [13])

k_{pv}	k_{iv}	k_{pi}	k_{ii}
0.52	1.161022	0.738891	1.19

TABLE VII: Parameters of SECM-3 and SECM-4 (values taken from [17] and [13])

Parameter	Value
k_{q}	5 pu
i_{thr}	0.92 pu
γ	$2.3\frac{p_{\text{base}}}{i_{\text{base}}}$ pu
p_{base}	4440 MW
i_{base}	$\frac{5300\text{MVA}}{15\text{kV}\sqrt{3}}$ A